JGR Space Physics

RESEARCH ARTICLE
10.1029/2019JA026776

Key Points:
- HIWIND-observed thermospheric winds tend to be equatorward during the morning hours
- Southward IMF B_z leads to more equatorward meridional winds in the morning
- TIEGCM runs predict poleward winds in the morning

Correspondence to:
Q. Wu,
qwu@ucar.edu

Citation:
Wu, Q., Knipp, D., Liu, J., Wang, W., Häggström, I., Jee, G., et al. (2019). What do the new 2018 HIWIND thermospheric wind observations tell us about high-latitude ion-neutral coupling during daytime? *Journal of Geophysical Research: Space Physics*, *124*, 6173–6181. https://doi.org/10.1029/2019JA026776

Received 28 MAR 2019
Accepted 8 JUN 2019
Accepted article online 22 JUN 2019
Published online 18 JUL 2019

What Do the New 2018 HIWIND Thermospheric Wind Observations Tell Us About High-Latitude Ion-Neutral Coupling During Daytime?

Qian Wu[1], Delores Knipp[1,2], Jing Liu[1], Wenbin Wang[1], Ingemar Häggström[3], Geonhwa Jee[4], Young-Sil Kwak[5], and Philip J. Erickson[6]

[1]High Altitude Observatory, National Center for Atmospheric Research, Boulder, CO, USA, [2]Smead Aerospace Engineering Sciences Department, University of Colorado, Boulder, USA, [3]EISCAT Scientific Association, Kiruna, Sweden, [4]Division of Polar Climate Change, Korea Polar Research Institute, Incheon, South Korea, [5]Space Science Division, Korea Astronomy and Space Science Institute, Daejeon, South Korea, [6]Haystack Observatory, Massachusetts Institute of Technology, Westford, MA, USA

Abstract Daytime thermospheric winds observed by the balloon-borne instrument HIWIND (High-altitude Interferometer WIND experiment) during two flights in June 2011 and 2018 from Kiruna (68°N, 20°E), along with simultaneous European Incoherent SCATter radar ion drift data, are analyzed. National Center for Atmospheric Research TIEGCM (Thermosphere Ionosphere Electrodynamics General Circulation Model) simulations for both flights are compared with observations. The observed thermospheric winds from the two flights have many similarities. HIWIND-observed thermospheric winds tend to be equatorward during the morning hours before noon and close to zero in the afternoon. In contrast, TIEGCM predicts poleward winds before noon and near zero in the afternoon. Southward interplanetary magnetic field B_z, occurring as the balloon passed through morning, was associated with greater equatorward meridional winds. The TIEGCM-simulated zonal winds have large differences with observations under more active conditions. The second HIWIND flight confirms some important results from the first flight and further shows thermospheric wind variations under different interplanetary magnetic field conditions. HIWIND observations in general provide invaluable data for model validation and highlight deficiencies in current high-latitude simulations.

1. Introduction

In spite of decades of high-latitude polar cap thermospheric wind observations from satellite-borne and ground-based instruments, there are still many unknowns about ion-neutral coupling processes in the region. In particular, we lack thermospheric wind observations in the summer, because the long daytime hours prevent ground-based Fabry Perot interferometers (FPIs) from observing thermospheric winds due to sunlight scattering. Advances in observation technology, combined with intense community interest in thermospheric winds and their variability, provide a compelling reason to revisit thermospheric wind measurements with improved fidelity and sensitivity. Earlier daytime observations of thermospheric winds were made by satellite instruments such as Dynamics Explorer-2 FPI, High Resolution Doppler Imager, and WIND Imaging Interferometer (Hays & Science Team, 1992; Killeen et al., 1982; Shepherd et al., 1993). Satellite-borne accelerometers were also used to derive cross-track winds in the thermosphere (e.g., Förster et al., 2008). We note that recent studies have shown that these wind observations may have a latitudinally dependent bias (Dhadly et al., 2018).

On 14 June 2011, the first balloon-borne FPI, HIWIND (High-altitude Interferometer WIND experiment), was launched from Kiruna, Sweden (68°N, 20°E). It is an instrument designed to observe thermospheric winds from balloon altitudes of ~40 km, where the sunlight scattering is only 0.1% of that on the ground. This enables O 630-nm redline dayglow thermospheric wind observations (Wu et al., 2012). During the 2011 flight, HIWIND revealed unexpected thermospheric wind features at high latitudes. In particular, on the dayside of the polar cap, the meridional winds were observed to be mostly equatorward, whereas the National Center for Atmospheric Research (NCAR) TIEGCM (Thermosphere Ionosphere Electrodynamics General Circulation Model) predicts poleward winds (Moe & Wu, 2014; Wu et al., 2012).

To explore the cause of observed equatorward thermospheric winds inside the polar cap, cusp heating and magnetospheric lobe cell convection effects were investigated (Sheng et al., 2015; Zhang et al., 2016). In these investigations, model simulations were able to reproduce equatorward winds on the dayside of the polar cap, consistent with HIWIND observations. Sheng et al. (2015) showed that this feature appeared after adding significant cusp heating in the model to bring the thermospheric wind equatorward. On the other hand, Zhang et al. (2016) were able to reproduce equatorward dayside winds in the simulations without adding heating in the cusp by using the CMIT (Coupled Magnetosphere Ionosphere Thermosphere) Model (Wiltberger et al., 2004). In that study, the positive interplanetary magnetic field (IMF) B_y component in combination with the northward IMF B_z condition produced a more compact and stronger magnetosphere duskside lobe convection cell in the CMIT. This resulted in equatorward dayside wind due to a stronger compact duskside lobe cell. Because the 2011 HIWIND data set was the only one available until recently, there were great uncertainties related to these studies due to their single case study nature, and it was unclear whether the thermospheric winds would be different under different IMF and geomagnetic conditions.

Recently, we have obtained another set of daytime thermospheric wind data from the June 2018 HIWIND flight, which affords us an opportunity to examine the daytime thermospheric winds in the polar cap under different IMF conditions. In this paper, we execute a one-to-one comparison of the 2011 and 2018 data sets to see how the thermospheric winds differ under different geomagnetic conditions. In addition to the HIWIND thermospheric wind observations, we also have colocated simultaneous EISCAT (European Incoherent SCATter) radar ion drift observations from Kiruna during the two flights. Furthermore, we also show TIEGCM simulations for both flights to see how model predictions perform under different geophysical conditions. We present observational data and simulations in the next section, which is followed by discussion of the results. Finally, we summarize our findings.

2. HIWIND and EISCAT Observations and TIEGCM Simulations

2.1. HIWIND Thermospheric Wind Observations

Wu et al. (2012) described the HIWIND instrument. It is a similar instrument to the Resolute FPI (Wu et al., 2004). HIWIND is enclosed in a pressure vessel, which maintains 1-atm pressure. It has a 10-cm aperture etalon with 2-cm gap and 80% reflectivity. The etalon chamber is sealed and maintains temperature stability of 0.1 °C with a heater and a temperature controller. The pressure inside the chamber is monitored. The instrument has a rotating mirror, which can point the instrument to four orthogonal directions with 40° elevation angle through four portholes. The integration time is 1 min. The zero-wind values are obtained by averaging observations from opposite viewing directions for each measurement cycle. The zero-wind values contain the instrument drift and vertical wind contribution. In this way, we do not assume the vertical wind equal to zero, because the vertical wind contribution to the measurement along with the instrument drift all removed once the zero-wind value is subtracted from the observations. However, it is assumed that the wind is uniform within the four measurement points roughly 500 km apart, which we also do for ground-based FPIs.

The HIWIND gondola is controlled by a National Aeronautics and Space Administration (NASA)-provided rotator, which compensates the balloon rotation during the flights and maintains the lock toward the Sun with stability better than ±1°, which can introduce about 4-m/s error for thermospheric wind of 200 m/s. The balloon speed and heading are measured by a GPS compass and recorded in the FPI data header. The balloon speed (~15 m/s) is removed during the data processing. The meridional and zonal winds are obtained by decomposing data from different orthogonal viewing directions of HIWIND based on the orientation of the gondola. The wind measurement errors mostly range from 15 to 30 m/s. The errors are intensity and background dependent.

The two balloon flights in June 2011 and 2018 (herein referred to as F2011 and F2018) started from Kiruna, Sweden, then drifted westward with stratospheric winds ranging from 10 to 15 m/s. Balloons usually take roughly 4 days to reach northern Canada. For F2011, we have data during the first 2 days before a power system failure stopped the observation. Therefore, although more data are available from F2018 following the first 2 days, no data from F2011 are available for comparison in that later period. Because of this limitation in the F2011 data set, we therefore compare only the first 2 days of the two flights in this initial study. The first 2 days for F2011 are 14 June, day of year (DOY) 165, and 15 June (DOY 166) 2011 (herein referred as

10.1029/2019JA026776

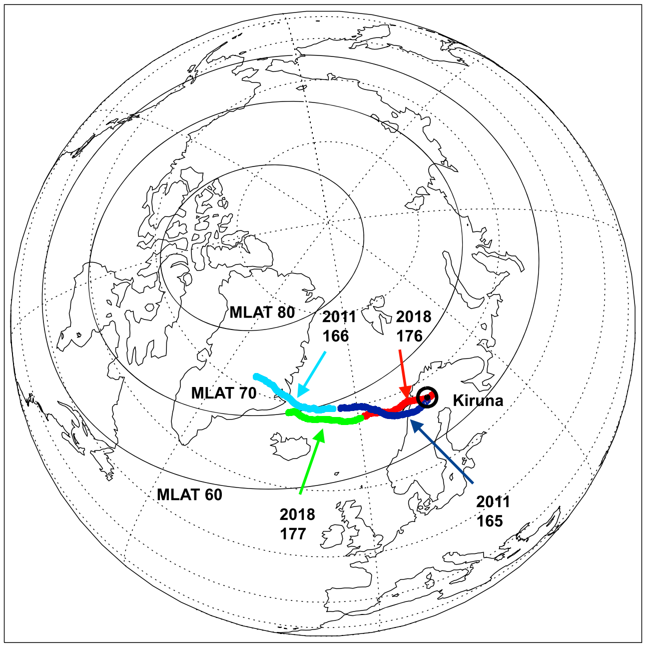

Figure 1. Balloon flight paths during the first 2 days of the two flights. The 2011 flight is shown in dark blue (14 June 2011, 2011165) and light blue (15 June 2011, 2011166). The 2018 flight is shown in red (25 June 2018, 2018176) and green (26 June 2018 2018177). The stratospheric winds during the 2011 flight were slightly faster than those during the 2018 flight.

2011165 and 2011166), whereas those for F2018 are 25 June (DOY 176) and 26 June (DOY 177) 2018 (herein, we refer them as 2018176 and 2018177). The balloon flight paths are plotted in Figure 1. The balloon paths of the two flights are similar, and the HIWIND balloon moved faster during F2011. Each day is marked by a different color. For reference, the values of the 10.7-cm wavelength (F10.7) solar output proxy index for 2011165, 2011166, 2018176, and 2018177 are 102.5, 104.8, 75.2, and 73.4 solar flux units (sfu), respectively, where 1 sfu = 10^{-22} W·m^{-2}·Hz^{-1}.

2.2. Kiruna/Tromsø EISCAT Ion Drift Observations

To obtain simultaneous ion drift data, we operated the EISCAT ultrahigh frequency incoherent scatter radar at Tromsø during both flights. The EISCAT radar was running a relatively narrow three-position scan, to enable ion drift estimates at altitudes in the *E* and *F* regions. The mode averages 5-min vector values over an area of about 50-km diameter in the *F* region and half that in the *E* region, to the west and south of the radar location in Tromsø, Norway. The basic range resolution is 3 km, the *F* region drift data are averaged from 160 to 350 km. In addition to the drifts, the basic incoherent scatter parameters, such as electron density, electron and ion temperatures were extracted along the individual beam directions.

2.3. TIEGCM Simulations

The TIEGCM is a first-principles model of the coupled thermosphere and ionosphere system (Richmond et al., 1992). The model solves the three-dimensional momentum, energy, and continuity equations of both the neutral and ionized gasses. The model also incorporates a self-consistent solution of the midlatitude and low-latitude dynamo. At its lower boundary (97 km), the model is driven by tidal forcing climatology from the Global Scale Wave Model (Hagan & Forbes, 2002, 2003). At high latitudes, we use the Weimer ion convection model (Weimer, 2005). In this study, we use the 1.25° × 1.25° high-resolution version of the TIEGCM (Dang et al., 2018). One-fourth scale height vertical grid is used. The high-resolution model allows us to track the model simulations along the balloon flight path better. The upper boundary of the model is at about 500-km altitude and solar activity dependent.

2.4. Observations on 2011165 and 2018176

The wind data for the first day of the two flights are plotted in Figure 2. The IMF data for the days are shown in Figure 3. IMF B_z had a brief southward excursion around 8 UT (9 LT) on 2011165 (marked by the first arrow). IMF B_z was mostly northward during the first half of 2018176 and turned southward after 1030 UT (marked by the second arrow). The meridional winds (positive poleward) from the two flights resemble each other, even though the data are 7 years apart, under different solar extreme ultraviolet conditions, and not on the same day of the year. We note a brief equatorward deviation of the meridional winds from 8 UT (~9 LT) to 11 UT on 2011165 (marked by the first arrow). This deviation is likely associated with the substorm activity due to the aforementioned short southward period of the IMF B_z component (Figure 3). The meridional winds of the two data sets had large differences, when the HIWIND balloon likely crossed the auroral oval after 20 UT (~21 LT). The meridional ion drift data from EISCAT also showed large differences between two flights around the same time. Overall, the 2018176 meridional winds show the tendency be mostly poleward with a speed of ~30 m/s from 8 to 18 UT (~9 to 19 LT), whereas the 2011165 data were mostly near zero from 11 UT to 18 UT. We should note that the daytime winds are in the rough order of measurement uncertainty. However, the tendency is consistent with multiple data points even with sizable error bars.

In contrast, the zonal wind (positive eastward) data of the two flights differ from each other at multiple points. Before 6 UT (~7 LT), both 2011165 and 2018176 data changed from near zero to more than 100 m/s in the westward direction. From 6 to 12 UT, the two data sets were nearly identical. At 1230 UT, the zonal ion drifts on 2018176 shifted westward and pulled the zonal neutral wind with it. On 2011165, the

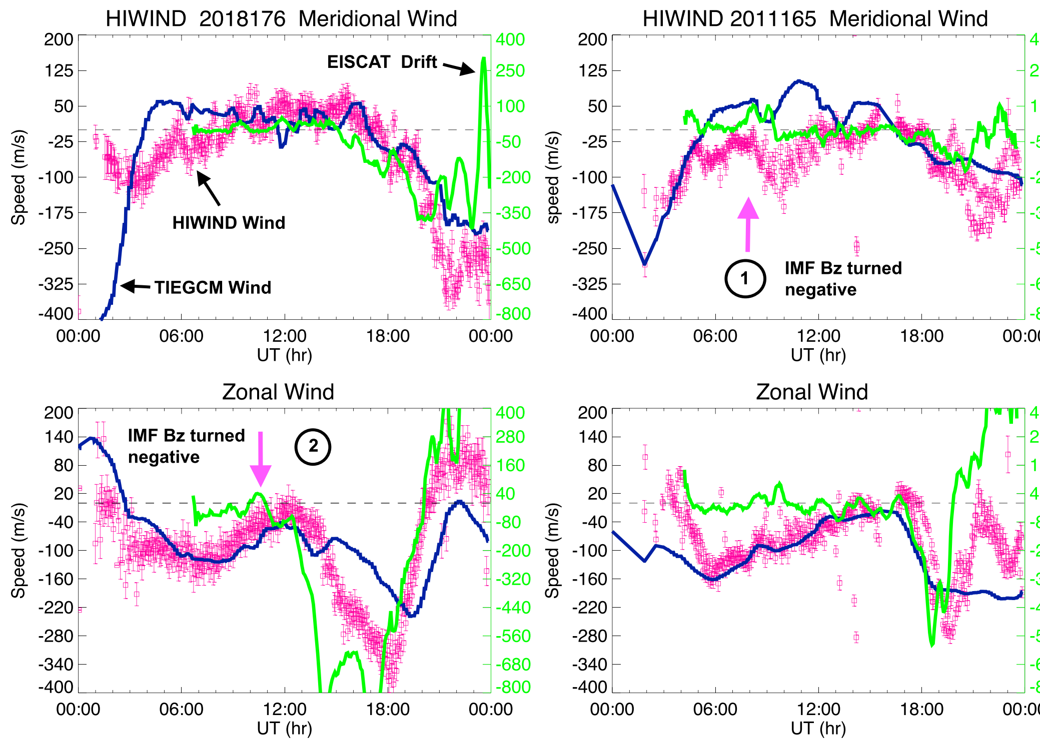

Figure 2. Observations and simulations for the first day of the 2018 (left) and 2011 (right) flights. The meridional (upper) and zonal (lower) components of thermospheric winds from HIWIND (pink dots), ion drifts from EISCAT radar (green), and TIEGCM-simulated winds (dark blue). The ion drift scale is on the right in meters per second, which is double the scale for the neutral winds. The wind errors for HIWIND observations range from 15 to 30 m/s. EISCAT = European Incoherent SCATter; HIWIND = High-altitude Interferometer WIND experiment; IMF = interplanetary magnetic field; TIEGCM = Thermosphere Ionosphere Electrodynamics General Circulation Model.

zonal ion drift stayed mostly zero until 17 UT, then it started to turn westward and dragged the neutral winds along. The differences in the zonal winds are most likely related to the difference in the onset time of the westward ion drifts, as well as the drift speeds. On 2018176, IMF B_z was negative since 1030 UT (marked by the second arrow) and remained so to the end of the day. On 2011165, IMF B_z was mostly positive during the latter half the day. The effect of IMF B_z on the zonal wind via the ion drifts was strong with a large westward acceleration, probably a reflection of a strong daytime ion-neutral interaction. Note that the ion drifts in the meridional direction were small and close to each other for these 2 days, so the ion drag effects on the meridional winds were small and did not produce large differences between the meridional winds of 2011165 and 2018176. Therefore, the changes of the zonal winds due to ion drag were different from those of the meridional winds. It is also possible that in the afternoon sector, the zonal direction was in line with the antisunward direction and changes in antisunward convection due to IMF B_z variations affect the zonal wind more.

2.5. TIEGCM Simulations for 2011165 and 2018176

The TIEGCM simulations are known to produce more poleward meridional winds on the dayside of the polar cap for 2011165 (Sheng et al., 2015; Wu et al., 2012; Zhang et al., 2016). We plot the TIEGCM simulations for 2011165 in Figure 2 for ease of comparison. A negative IMF B_y tends to make the two ion convection cells about equal size. A positive IMF B_y, on the other hand, leads to a larger duskside convection cell (e.g., Weimer, 2005). Consequently, the converging zone of the two cells, where the poleward ion drift enhances, tends to be shifted toward dawn by a positive IMF B_y and more or less stays in the middle close to the noon under negative IMF B_y conditions. Because during 2018176, IMF B_y was negative, we may have had the convergence zone located close to noon, leading to stronger poleward winds as shown by HIWIND meridional wind observations. We note however that this is only one possibility for IMF B_y influence. In general, TIEGCM simulations of 2011165 and 2018176 periods do not always agree with the data. The TIEGCM-

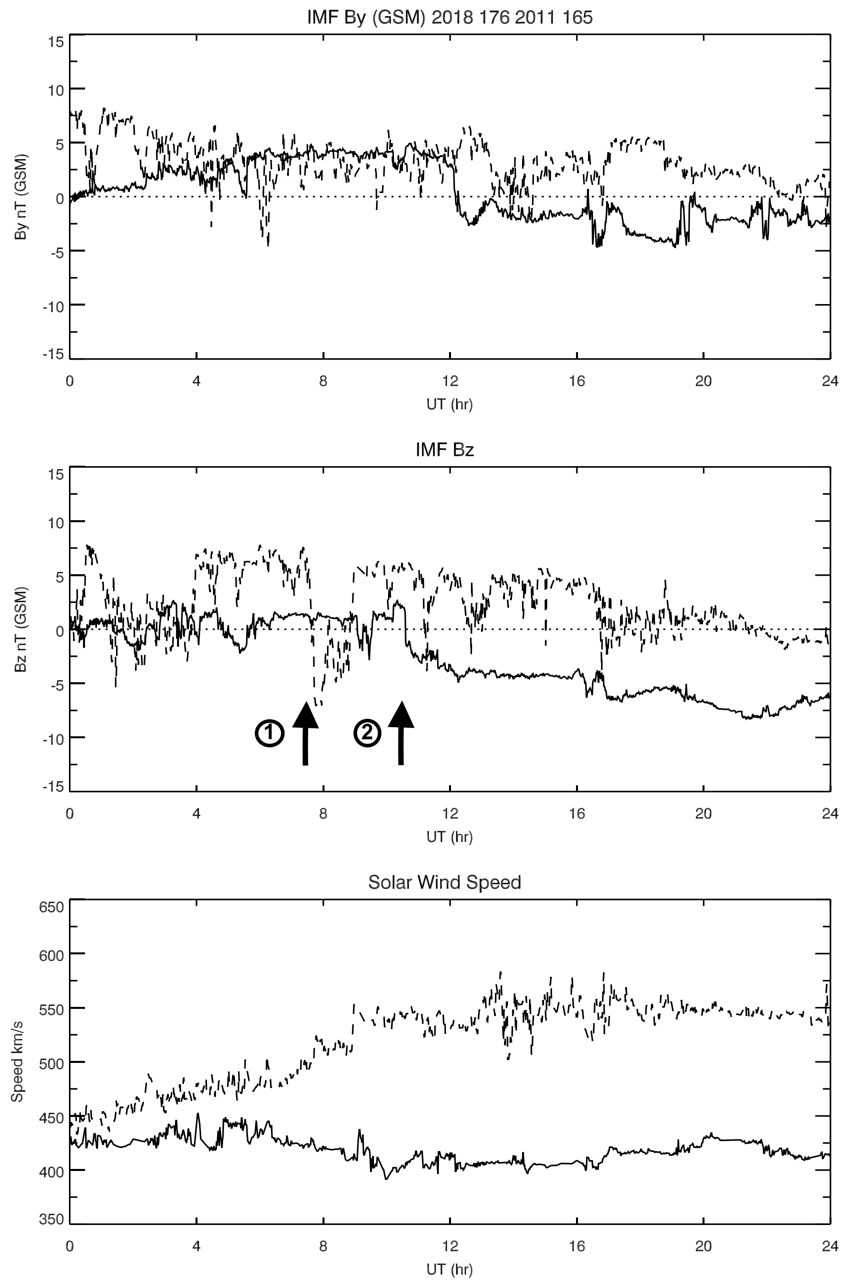

Figure 3. IMF conditions for the first day of the two flights. The IMF B_y and B_z components and solar wind speed for 2011165 (dashed) and 2018176 (solid) are plotted. Two southward turning of IMF B_z are marked by two arrows. The first for F2011 and the second for F2018. GSM = geocentric solar magnetospheric; IMF = interplanetary magnetic field.

simulated meridional winds for 2011165 are poleward with a speed between 0 and 50 m/s from 10 to 15 UT. On the other hand, for 2018176, model and data compared reasonably well between 10 and 20 UT, although there are discrepancies in the temporal variations. Beyond IMF B_y, we look at the IMF B_z component.

On 2011165, IMF B_z was positive but for 2018176 IMF B_z was negative after 9 UT (10 LT). A positive IMF B_z on 2011165 should produce weak antisunward (poleward) convection. Yet the TIEGCM predicted stronger poleward winds for 2011165. This shows the difficulty the TIEGCM is facing on the dayside polar cap due to its use of empirical ion convection patterns rather than actual convection on the day in question. Some model observation discrepancies are common for both 2011165 and 2018176. For example, before 9 UT (~10 LT), the simulations for both 2011165 and 2018176 are poleward, whereas the HIWIND observations were equatorward.

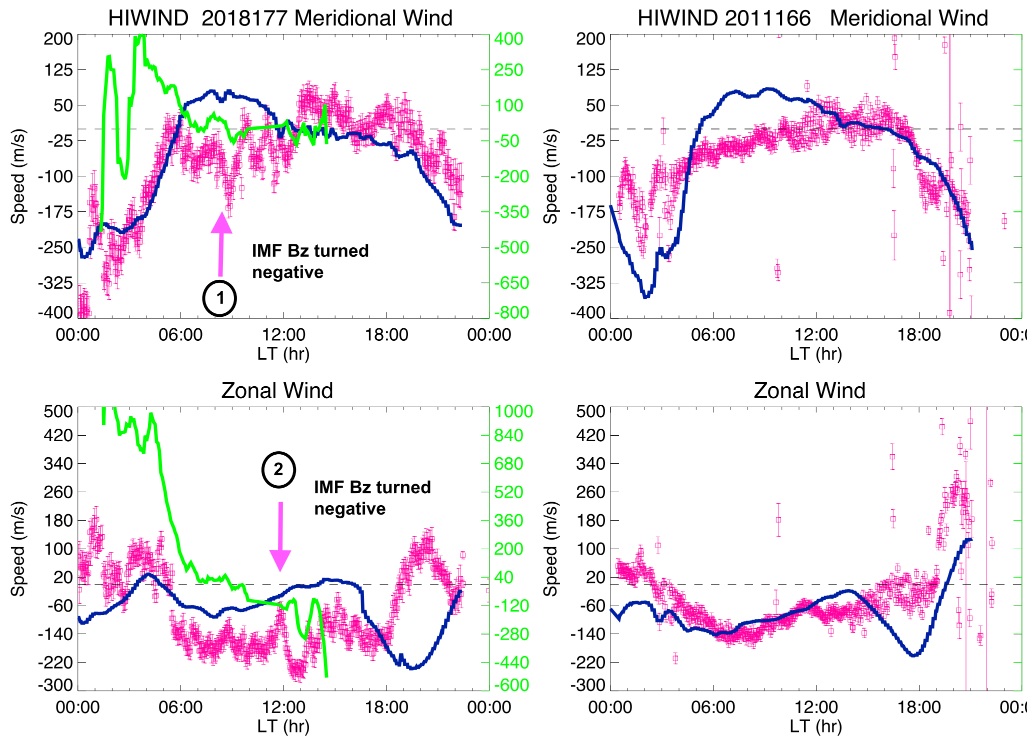

Figure 4. Same as Figure 2 but for the second day of the two flights 2011166 and 2018177. HIWIND = High-altitude Interferometer WIND experiment; IMF = interplanetary magnetic field.

While model-data comparison for the meridional winds for 2011165 looks worse than that for 2018176, the comparison for zonal winds reaches an opposite conclusion. The TIEGCM simulations of the zonal winds for 2011165 mostly follow the observed zonal winds, except at the beginning and end of the day, when HIWIND was very close to the auroral oval. Being close to the auroral oval is problematic for the TIEGCM simulations, because the model uses not only an empirical ion convection model but also an empirical auroral oval model, which does not always represent the real auroral oval well. The electric field near the auroral oval is highly variable and difficult to model. In the case of 2018176, the observed zonal winds turned westward after 12 UT, because IMF B_z turned southward a little earlier. The TIEGCM-simulated westward zonal winds are much weaker than those of the HIWIND observations after 15 UT.

2.6. Observations on 2011166 and 2018177

The HIWIND data for 2011166 and 2018177 are displayed in Figure 4 and IMF parameters in Figure 5. In this case, we show the data in local time for better comparison, since the balloon paths for the two flights have larger differences in the second day than in the first day, as shown in Figure 1. By plotting them in local time, we align the data to emphasize local time variations. Note that LT roughly equals UT − 2 for 2011166 and UT − 1 for 2018177, because the HIWIND balloon speed was lower during F2018. Only F2018 has ion drift data. Furthermore, given the larger distance between the balloon and the EISCAT radar site after flying 1 day, the EISCAT and HIWIND were no longer colocated. Overall, the meridional winds of 2011166 and 2018177 are not very different from each other. The 2018177 data also have more temporal variations, which is not surprising given that the IMF on 2018177 had stronger variations compared to that on 2011165.

There was an equatorward excursion around 10 LT on 2018177 in the meridional winds (marked by the first arrow) similar to that around the same time in 2011165, which is likely related to the IMF B_z southward period (marked by the first arrow) in Figure 5. The zonal winds on 2018177 were mostly eastward until 5 LT and turned westward quickly. The 2018177 zonal winds had stronger temporal variations than those of the 2011166. Some of which are likely related to the IMF variations in both B_y and B_z (Figure 5). We marked the time of another southward turning in IMF B_z at ~13 UT and the possible response in the zonal wind (~12 LT) with the second arrow in Figures 4 and 5.

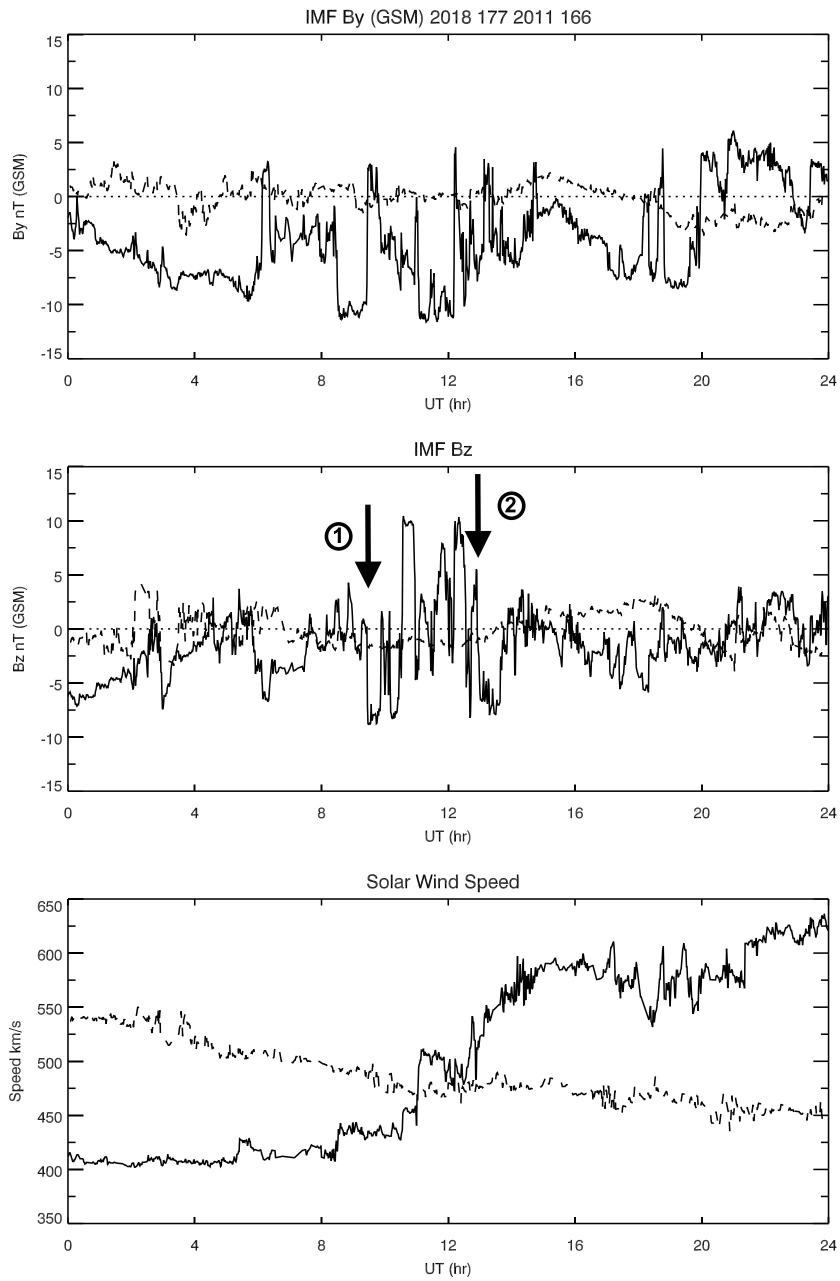

Figure 5. Same as Figure 3 but for the second day of the two flights. Two southward turnings of IMF B_Z in the F2018 flight are marked by two arrows. GSM = geocentric solar magnetospheric; IMF = interplanetary magnetic field.

The 2018177 ion drift was strongly eastward and later close to zero after 6 LT. The zonal ion drift changed from strongly eastward to close zero simultaneously as the neutral wind turned westward. We do not see the ion drifts turning westward before 9 LT, probably because EISCAT radar at this time was far east of the HIWIND balloon and its observations were no longer representative of the local ion drifts for HIWIND. However, the EISCAT observations near Kiruna do indicate that the ion drifts were turning toward westward after 10 LT.

2.7. TIEGCM Simulations for 2011166 and 2018177

The TIEGCM modeled winds are sampled along the balloon path during F2011 and F2018 and plotted in Figure 4. The simulated meridional winds on 2011166 and 2018177 are very similar. There are large model versus observation discrepancies in meridional winds for both 2011166 and 2018177 between 6 and 12 LT. The model predicts poleward winds, whereas the observed winds were mostly equatorward. IMF B_z had more negative periods in 2018177. Consequently, 2018177 was geomagnetically more active. The TIEGCM-simulated meridional winds gradually converge to the observed winds after 12 LT. The simulated zonal winds match the observation better in 2011166. The observed westward zonal winds in 2018177 were stronger than those in 2011165 between 12 and 18 LT, whereas the simulated zonal winds were opposite, with larger westward speeds in 2011166.

3. Discussion

By comparing the observations from the two balloon flights, we show thermospheric winds observed approximately at the same location and same season but under different geomagnetic and solar extreme ultraviolet radiation conditions. It is striking that there are many similarities between the two data sets even though they are 7 years apart. The differences in the thermospheric winds seen in the data sets examined are likely related to the solar wind and IMF conditions. Compared to the nighttime thermospheric winds, the daytime thermospheric winds seem to have more similar patterns. This is reasonable considering that the daytime thermosphere, with higher density and larger ion drag, is less mobile than the nighttime thermosphere. During the nighttime, the thermospheric winds are less constrained, leading to higher variability.

In some ways, however, our view of the thermospheric winds may be biased by the fact that past thermospheric wind observations occurred primarily at night due to ground-based instrumental limitations. Most of our daytime thermospheric observations were made by satellites, which do not repeat themselves at the same location and same local time at high latitudes compared to ground-based observations. In general, daytime observations of HIWIND, occurring at nearly the same local times and same locations, make comparisons of winds under different conditions easier, and indeed this platform's capabilities allow the direct observation that daytime thermospheric winds seem to be less variable than the nighttime winds.

The TIEGCM simulations provide some clues to the relationship of thermospheric wind variation to IMF conditions. However, model-data differences remain significant. In particular, dayside meridional winds from the simulations still have the tendency to be more poleward than the observations, mostly before noon. (The agreement in the afternoon is better.) The simulated zonal winds have large differences with the observations during geomagnetically active periods for both 2018176 and 2018177. Model-observation discrepancy in meridional winds may be related to cusp heating. Specifically, satellite thermospheric density observations have shown a density bulge near the cusp, which may be related to cusp heating (e.g., Deng et al., 2013; Moe & Wu, 2014; Zhang et al., 2015). Such a density bulge may change the local pressure gradient to produce equatorward wind at the latitudes sampled by HIWIND. Results of these comparisons also indicate that there remains a need to drive the TIEGCM directly with magnetospheric inputs like CMIT to see how different lobe cell configuration may impact the thermospheric winds. In particular, Zhang et al. (2016) showed that the Weimer convection model gives a very large duskside convection cell under large positive IMF B_y conditions. Consequently, the return flow on the duskside is not strong enough to overcome the pressure gradient across the sunlight terminator to force an equatorward flow on the dayside. In the case of CMIT simulation the duskside convection cell is much smaller and stronger. As a result, the return flow of the duskside cell pushes the neutrals equatorward on the dayside (Figure 3a in Zhang et al., 2016).

Further analysis of HIWIND data is planned. In particular, since the HIWIND 2018 flight occurred very recently, we do not have more sophisticated model runs from the CMIT yet, which require more computational time. We look forward to direct magnetospheric ion convection-driven model simulations for the two HIWIND flights under different IMF conditions. We anticipate that the results of these comparisons will be very significant for not only model validation but for better understanding of high-latitude ion neutral coupling and ion convection morphology.

4. Summary

We compare the HIWIND observations from F2011 and F2018 with the primary goal of examining effects of solar wind and IMF conditions on the polar cap thermospheric winds during the summer season. Our findings can be summarized as

1. The observed thermospheric winds from the two flights have many similarities.
2. HIWIND-observed thermospheric winds tend to be equatorward during the morning hours before noon and close to zero in the afternoon. By contrast, TIEGCM runs predict poleward winds before noon and near zero in the afternoon.
3. Occurrence of southward IMF B_z conditions as the balloon passes through the morning appears to lead to more equatorward meridional winds.
4. TIEGCM-simulated zonal winds have large differences with observations under more active conditions.

Overall, the second HIWIND flight confirms some important results from the first flight and shows thermospheric wind variations under different IMF conditions. More importantly, we have demonstrated that the HIWIND instrument provides invaluable data for model validation and in particular can highlight deficiencies in current high-latitude simulations. Two flights are certainly not sufficient to tackle all unknowns related to high-latitude ion-neutral coupling, which are critically important to space weather and aeronomy in general. Due to this need, we plan to pursue additional HIWIND flights in the future.

Acknowledgments

The HIWIND project is supported by NASA Grant NNX15AK75G. NCAR is supported by the National Science Foundation. Q. W. is also supported by NASA Grant NNX17AG69G. W. W. and J. L. are supported in part by NASA Grants NNX14AE06G, NNX15AB83G, NNX17AI42G, and 80NSSC17K0013. D. J. K. is supported by AFOSR Grant FA9550-17-1-0258. EISCAT is an international association supported by research organizations in China (CRIRP), Finland (SA), Japan (NIPR and STEL), Norway (NFR), Sweden (VR), and the United Kingdom (NERC). EISCAT ISR radar observations were supported by the EISCAT peer review program, Korean Polar Research Institute (PE19020), and basic research funding from Korea Astronomy and Space Science Institute. The HIWIND payload is designed and constructed by NCAR HAO Instrument Group, NCAR EOL Design and Fabrication Services, Sierra Scientific Solutions Inc, ExtractCraft LLC, and FabCon LLC. Engineering efforts by Scott Sewell, Alice Lecinski, Nicole Ela, Rob Grave, Pete Nelson, Lee Sutherland, Bart Woodiel, and Peter Yee are gratefully acknowledged. NASA Columbia Scientific Balloon Facility provided balloon launch service and facilitate HIWIND project in many other ways. The HIWIND and TIEGCM simulation data are available at doi:10.5065/4GER-3779 (https://www2.hao.ucar.edu/data-supporting-publication-what-do-new-2018-hiwind-daytime-thermospheric-wind-observations-tell-us). The EISCAT data are available from the Madrigal Database (http://millstone-hill.haystack.mit.edu/).

References

Dang, T., Lei, J., Wang, W., Burns, A., Zhang, B., & Zhang, S.-R. (2018). Suppression of the polar tongue of ionization during the 21 August 2017 solar eclipse. *Geophysical Research Letters*, *45*(7), 2918–2925. https://doi.org/10.1002/2018GL077328

Deng, Y., Fuller-Rowell, T. J., Ridley, A. J., Knipp, D., & Lopez, R. E. (2013). Theoretical study: Influence of different energy sources on the cusp neutral density enhancement. *Journal of Geophysical Research: Space Physics*, *118*, 2340–2349. https://doi.org/10.1002/jgra.50197

Dhadly, M. S., Emmert, J. T., Drob, D. P., Conde, M. G., Doornbos, E., Shepherd, G. G., & Ridley, A. J. (2018). Seasonal dependence of geomagnetic active-time northern high-latitude upper thermospheric winds. *Journal of Geophysical Research: Space Physics*, *123*, 739–754. https://doi.org/10.1002/2017JA024715

Förster, M., Rentz, S., Liu, H., & Haaland, S. E. (2008). IMF dependence of high-latitude thermospheric wind pattern derived from CHAMP cross-track measurements. *Annales de Geophysique*, *26*(6), 1581–1595. https://doi.org/10.5194/angeo-26-1581-2008

Hagan, M. E., & Forbes, J. M. (2002). Migrating and nonmigrating diurnal tides in the middle and upper atmosphere excited by tropospheric latent heat release. *Journal of Geophysical Research*, *107*(D24), 4754. https://doi.org/10.1029/2001JD001236

Hagan, M. E., & Forbes, J. M. (2003). Migrating and nonmigrating semidiurnal tides in the upper atmosphere excited by tropospheric latent heat release. *Journal of Geophysical Research*, *108*(A2), 1062. https://doi.org/10.1029/2002JA009466

Hays, P. B., & HRDI Science Team (1992). Remote sensing of mesospheric winds with the High-Resolution Doppler Imager. *Planetary and Space Science*, *40*(12), 1599–1606. https://doi.org/10.1016/0032-0633(92)90119-9. Hedin

Killeen, T. L., Hays, P. B., Spencer, N. W., & Wharton, L. E. (1982). Neutral winds in the polar thermosphere as measured from Dynamics Explorer. *Geophysical Research Letters*, *9*(9), 957–960. https://doi.org/10.1029/GL009i009p00957

Moe, K., & Wu, Q. (2014). Impact of HIWIND balloon measurements on thermospheric density models. *Journal of Geophysical Research: Space Physics*, *119*, 2476–2483. https://doi.org/10.1002/2013JA019390

Richmond, A. D., Ridley, E. C., & Roble, R. G. (1992). A thermosphere/ionosphere general circulation model with coupled electrodynamics. *Geophysical Research Letters*, *19*(6), 601–604. https://doi.org/10.1029/92GL00401

Sheng, C., Deng, Y., Wu, Q., Ridley, A., & Häggström, I. (2015). Thermospheric winds around the cusp region. *Journal of Geophysical Research: Space Physics*, *120*, 1248–1255. https://doi.org/10.1002/2014JA020028

Shepherd, G. G., Thuillier, G., Gault, W. A., Solheim, B. H., Hersom, C., Alunni, J. M., et al. (1993). WINDII, the Wind imaging interferometer on the Upper Atmosphere Research Satellite. *Journal of Geophysical Research*, *98*(D6), 10,725–10,750. https://doi.org/10.1029/93JD00227

Weimer, D. R. (2005). Improved ionospheric electrodynamic models and application to calculating Joule heating rates. *Journal of Geophysical Research*, *110*, A05306. https://doi.org/10.1029/2004JA010884

Wiltberger, M., Wang, W., Burns, A. G., Solomon, S. C., Lyon, J. G., & Goodrich, C. C. (2004). Initial results from the coupled magnetosphere ionosphere thermosphere model: Magnetospheric and ionospheric responses. *Journal of Atmospheric and Solar - Terrestrial Physics*, *66*(15–16), 1411–1423. https://doi.org/10.1016/j.jastp.2004.03.026

Wu, Q., Gablehouse, R. D., Solomon, S. C., Killeen, T. L., & She, C.-Y. (2004). A new Fabry-Perot interferometer for upper atmosphere research. *Proceeding SPIE 5660, Instruments, Science Methods Geospatial Planet Remote Sensing*, *218*. https://doi.org/10.1117/12.573084

Wu, Q., Wang, W., Roble, R. G., Häggström, I., & Strømme, A. (2012). First daytime thermospheric wind observation from a balloon-borne Fabry-Perot interferometer over Kiruna (68N). *Geophysical Research Letters*, *39*, L14104. https://doi.org/10.1029/2012GL052533

Zhang, B., Varney, R. H., Lotko, W., Brambles, O. J., Wang, W., Lei, J., et al. (2015). Pathways of *F* region thermospheric mass density enhancement via soft electron precipitation. *Journal of Geophysical Research: Space Physics*, *120*, 5824–5831. https://doi.org/10.1002/2015JA020999

Zhang, B., Wang, W., Wu, Q., Knipp, D., Kilcommons, L., Brambles, O. J., et al. (2016). Effects of magnetospheric lobe cell convection on dayside upper thermospheric winds at high latitudes. *Geophysical Research Letters*, *43*, 8348–8355. https://doi.org/10.1002/2016GL069834